Risley Prism Scan Patterns

Gerald F. Marshall, Consultant in Optics[1]
410 Dusenbury Street, Niles, Michigan 49120-1468

ABSTRACT

The Risley optical scanning system[Ref:1,2] consists of two sequential wedge prisms, which have wedge angles A_1 and A_2, that are capable of rotating about the optical scan axis at angular speeds ω_1 and ω_2. When a focussed laser beam is directed along the optical scan axis and through the prisms, the emergent beam is deviated in a direction according to the relative orientation of the prisms with respect to each other. When the individual prisms are rotated clockwise or counterclockwise, the combined deviation angle and the orientation phase change with time, such that the image spot traces out a vector pattern. This paper presents an interesting set of generated scan patterns that include regular polygons by selecting particular values for the ratios of A_2/A_1 and ω_2/ω_1.

Keywords: Scanner, Lissajous Figure, Risley prism, wedge prism.

1. INTRODUCTION

The Risley Prism is a pair of wedge prisms in tandem that are each separately capable of rotating about a common axis at different speeds, clockwise or counterclockwise to produce a variable prism power[2] with time. When a focussed laser beam is directed along the optical scan axis and through the pair of wedge prisms, the emergent beam is deviated in a direction according to the relative orientation — namely, the phase angle ϕ — of the prisms with respect to each other. and the resultant effective refracting angle and power of the Risley Prism (Figure 1.). The same patterns can be achieved with a pair of nutating mirrors in series.

Given: Refractive index of prism material = n
Then for small prism wedge angles the deviation angle D of a single wedge prism ≈ (n-1)A
When: n = 1.5; $\mathbf{D_1} = \mathbf{A_1}/2$; $\mathbf{D_2} = \mathbf{A_2}/2$; **D** = Vector addition of the deviations of prisms 1 and 2.

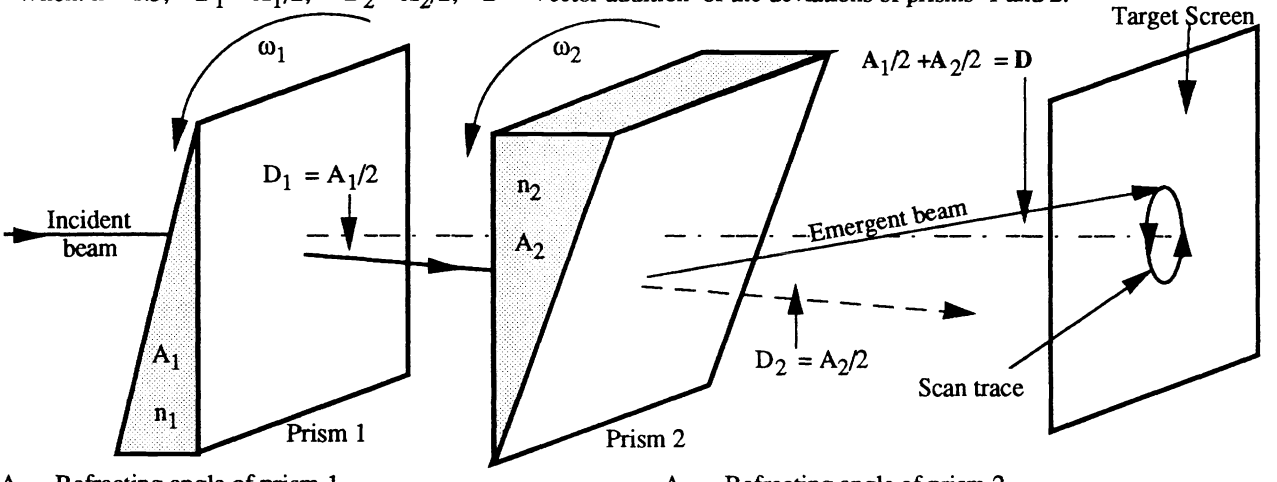

A_1 = Refracting angle of prism 1 .
A_2 = Refracting angle of prism 2.
D_1 = angle of deviation of the emergent beam from prism 1.
D_2 = angle of deviation of the emergent beam from prism 2.

Figure 1. Risley Prism scanner is composed of two wedge prisms capable of rotating about a common axis. Prism 2 can rotate either clockwise or counterclockwise with respect to wedge prism 1. The ratios A_2/A_1 and ω_2/ω_1 are represented by **k** and **M** respectively.

---

1. E-mail: marshallgf@aol.com; Telephone: (616) 687 1694; Fax: (616) 687 1693

2. The power of a prism is defined as the deflection of a beam measured in centimeters at a distance of one meter, in which case the unit of prism power is the *prism diopter*.

Part of the SPIE Conference on Optical Scanning: Design and Application
Denver, Colorado • July 1999 SPIE Vol. 3787 • 0277-786X/99/$10.00

1.1 Objective

This paper presents visibility to the effect of sequential discrete changes in parameters to produce a logical range of scan patterns. These patterns are achieved by selecting the different ratios for the wedge prisms' refracting angles **A** and their angular rotation speeds ω. The patterns include regular "polycusps" and polygons.

2. PROCEDURE

Consider that Prism 1 has a fixed refracting angle $\mathbf{A}_1$ and rotates at a fixed arbitrary angular speed ω_1 (Figure 1). Let $\mathbf{A}_2$ and ω_2 be variable parameters of prism 2, such that the ratios A_2/A_1 and ω_2/ω_1 are represented by **k** and **M** respectively. Further, let Prism 2 have an initial phase ϕ with respect to Prism 1.

2.1. Cartesian Equations of Scan Patterns.

When symbols **A** and **D** are printed in bold letters they represent vectorial quantities. This does not apply to other symbols shown in bold for visibility.

Let $\mathbf{D}_1$ and $\mathbf{D}_2$ represent the beam's vectorial angular deviations of Prism 1 and Prism 2 respectively.
Let **D** represent the vectorial addition of $\mathbf{D}_1$ and $\mathbf{D}_2$.
Then:

Deviation of the beam emerging from Prism 1	$\mathbf{D}_1 = \mathbf{A}_1(n-1)$	(1)
Deviation of the beam emerging from Prism 2	$\mathbf{D}_2 = \mathbf{A}_2(n-1)$	(2)
Let the ratio of the rotation speeds be	$\omega_2/\omega_1 = \mathbf{M}$	(3)
Let the ratio of the beam deviations be	$D_2/D_1 = \mathbf{k}$	(4)
Thus from equation (1)	$\mathbf{k} = A_2/A_1$	(5)

Hence the x and y vector components of D at a time **t** are given by

$$\mathbf{D}_x = \mathbf{D}_1\cos(\omega_1 t)+\mathbf{D}_2\cos(\omega_2 t-\phi) \quad (6)$$

$$\mathbf{D}_y = \mathbf{D}_1\sin(\omega_1 t)+\mathbf{D}_2\sin(\omega_2 t-\phi) \quad (7)$$

Figures 2. though 11. are a series of scan patterns produced by graphing $\mathbf{D}_y$ against $\mathbf{D}_x$.

2.2. Nomenclature of the Figures

Figures 2. though 11. show 4x3 matrices of scan patterns, that is, matrices of four rows by three columns; except that Figure 4. and Figure 9. are 2x3 matrices. A subFigure is referenced by its position in the matrix. For example in Figure 2. the subFigure in the top left hand conner is defined as Figure 2.1.1., while the subFigure in the bottom right hand conner is defined as Figure 2.4.3.

2.3 Figures

The following five pages, Sections **3.** are Figures 2. through 6. Each Figure contains scan patterns produced when the two wedge prisms rotate in the same direction with selected ratios **M**. As they rotate in the same direction the ratio of **M** has a positive value.

The succeeding following five pages, Sections **4.** are Figures 7. through 11. Each Figure contains scan patterns produced when the two wedge prisms rotate in opposite directions with selected ratios **M** and **k**. As they rotate in the opposite directions the ratio of **M** has a negative value.

At an appropriate time it is instructive to compare the corresponding figures and scan patterns in **Sections 3** and **4**.

3. POSITIVE VALUES OF M

Figures 2. through 6. only exhibit positive value of the ratio **M**; this means that Prism 1 and Prism 2 are both rotating in the same direction. **N** represents the number of complete rotations of Prism 1.

3.1. Circles

M =+1

k = +0, +0.5, +1

$\phi = 0°$

$\phi = 45°$

$\phi = 90°$

$\phi = 180°$

N = 1

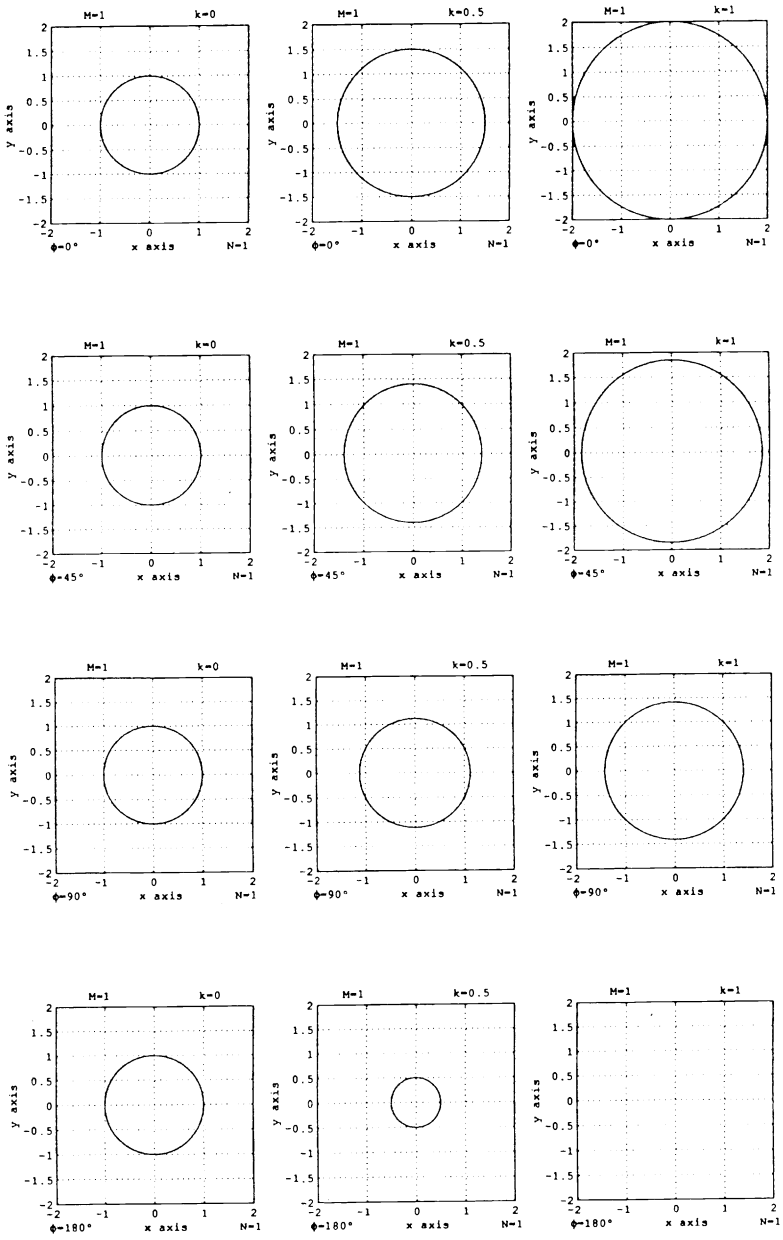

Figure 2. The four rows show the effect of changing the phase ϕ from zero degree, 45°, 90°, 180°. N=1.
The three columns show the effect of changing the ratio **k** from zero, 0.5 and 1.
Column 1 depicts scan patterns that are identical because **k** = zero. In effect Prism 2 is simply a parallel window that produces no angular deviation although it will produce a displacement of the emergent beam according to the window's thickness.
Column 2 depicts scan patterns that are decreasing in size as the phase ϕ increases, for **k**= 0.5.
Column 3 depicts scan patterns that are decreasing in size down to nothing as the phase ϕ is increased to 180°, for **k**= 1. The two angular deviations of Prism 1 and Prism 2 are in direct opposition and, therefore, cancel each other out. See also Figure 7.

3.2. Internal Loops

The upper set of six subFigures depicts scan patterns for integral steps of **M**, ranging from **M** = +1 through +6. The number of internal loops is in direct proportion to the numerical value of |**M**-1|. The size of the internal loops depends on the value of **k**. Compare with Figure 8.

M = 1, 2, 3, 4, 5, 6

$\phi = 0°$

k = 0.7

N = 1

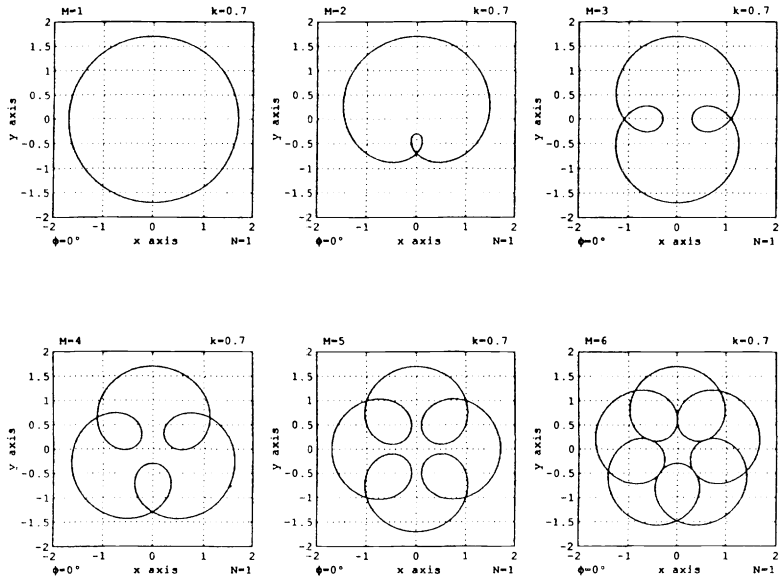

M = 1.1, 2.1, 3.1, 4.1, 5.1, 6.1

$\phi = 0°$

k = 0.7

N = 5

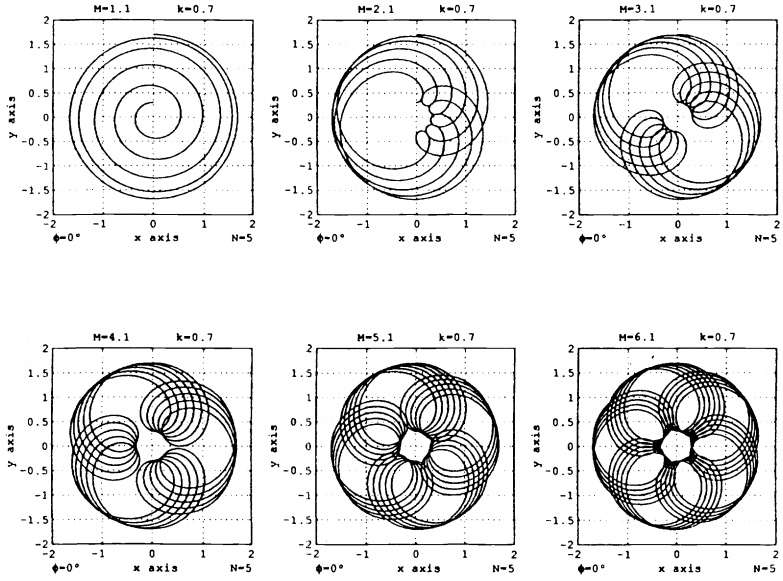

Figure 3. In each of the lowermost scan patterns **M** is increased by 10% to range non integrally from 1.1 through 6.6. Figures 3.3.1 through 3.4.3 with scan pattern have non integral values of **M**. With **N** = 5 the scan patterns rotate through **N** cycles. Because the patterns repeat themselves whenever the product |**M***N| is an integer the irradiance of the pattern increases towards the center of the doughnut shape of the scan patterns. The value of **M** needs to have a number with a recurring decimal for a smooth irradiance gradient.

It will be observed that the number of loops **L** is one digit less than the numerical value of **M**, that is, **L** = |**M**-1|.

3.3. Evolution of internal regular polycusps and polygons

Polycusps are defined as two-dimensional geometrical figures that have multiple cusps.

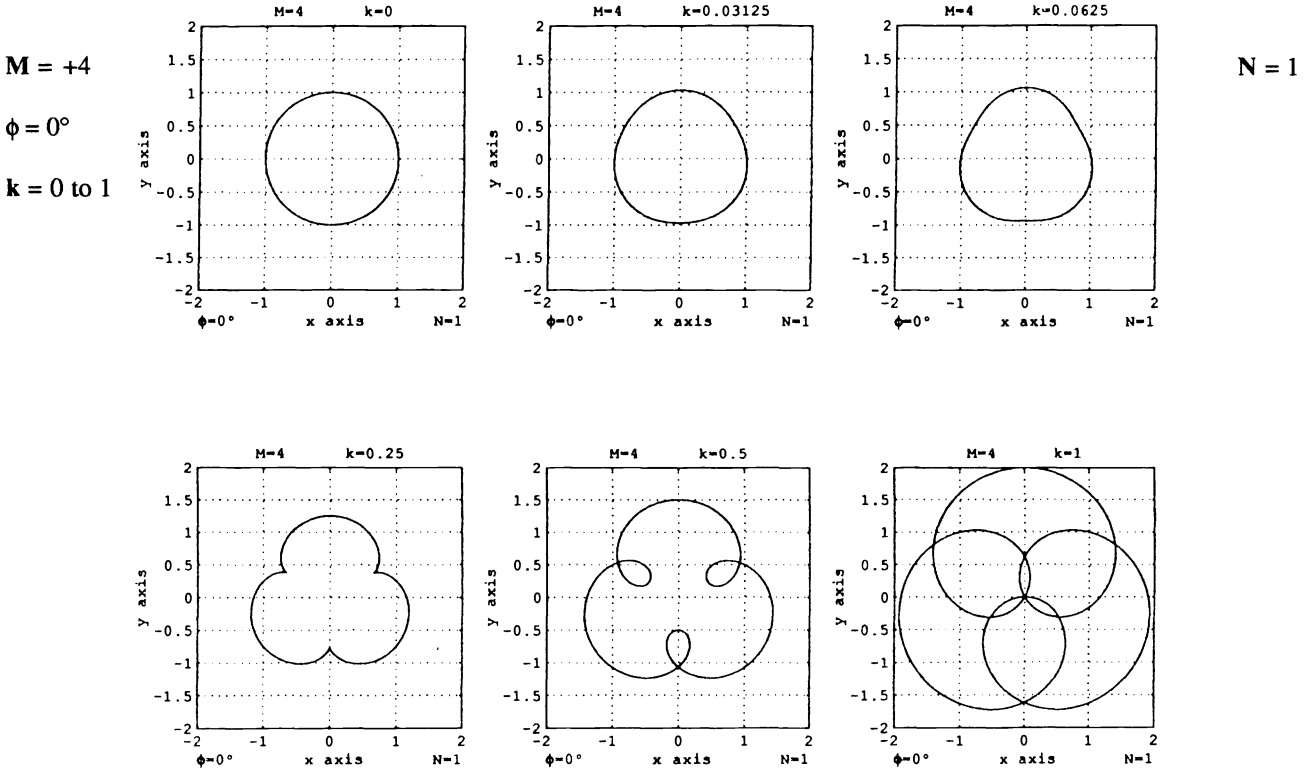

Figure 4. In each of the six subFigures **k** progressively ranges from zero to 1.

Figure 4.1.1. in which **k** = 0, the resultant scan pattern is understandably a circle as Prism 2 is simply a parallel window.

Figure 4.1.2. As **k** numerically increases the scan pattern changes to an egg shape.

Figure 4.1.3. As **k** continues to increase the scan pattern changes to a pear shape, with a suggestion of it being a triangle.

Figure 4.2.1. When **k** = 0.25 the resultant scan pattern has the distinct shape of a clover leaf with three sharp internal cusps.

Thence in:

Figure 4.2.2. When **k** = 0.5 three internal loops develop out of the cusps; the size of the loops depends on the value **k** > 0.5.

Figure 4.2.3. in which **k** = 1, the three internal larger loops intersect at the center of the scan pattern. It will be noticed that the number of cusps **C** and loops **L** is one digit less than the numerical value of **M**, that is, **C** = **L** = |**M**-1| as in Figure 3. Mathematical analysis shows that internal cusps are formed when **k** =1/±**M**. Compare with Figure 9.

3.4. Internal regular polycusps

In each of the uppermost six subFigures **M** ranges integrally from 1 through 6, while **k** = $[-1]^{M}(1/M)$. The term $[-1]^{M}$ orients each subFigure scan pattern to ensure there is a cusp at the bottom on the centerline.

M = 1, 2, 3,
4, 5, 6

$\phi = 0°$

k = -1, +0.5, -0.33•
0.25, -0.2, 0.166•

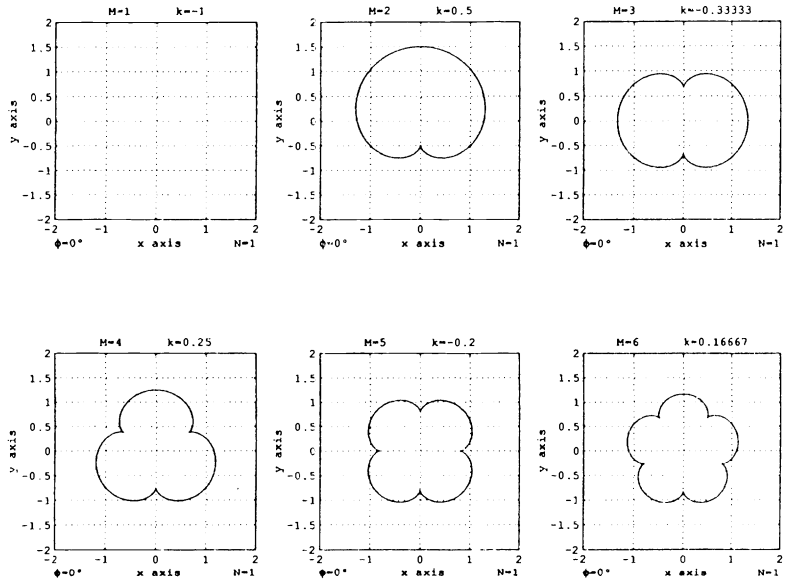

N = 1

M = 1.1, 2.2, 3.3
4.4, 5.5, 6.6

$\phi = 0°$

k = -1, +0.5, -0.33•
0.25, -0.2, 0.166•

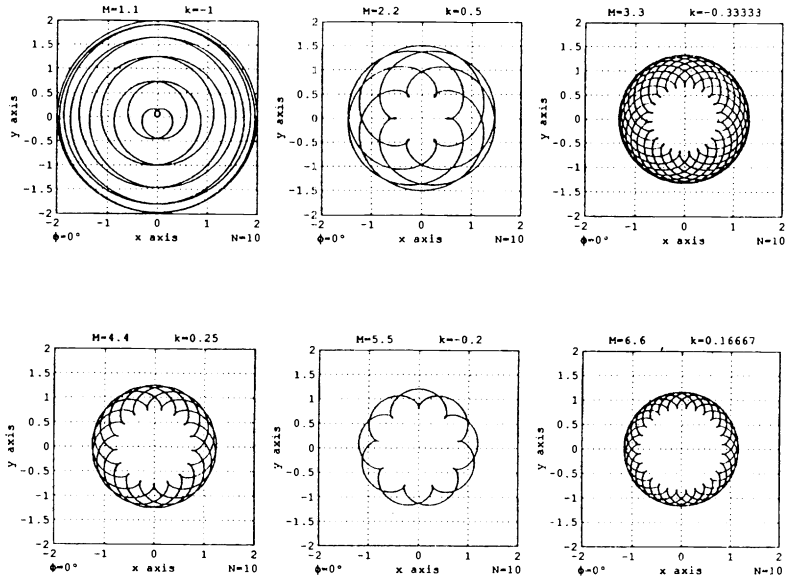

N = 10

Figure 5. In each of the lowermost scan patterns **M** is increased by 10% to range non integrally from 1.1 through 6.6.
Figure 5.1.1. has no scan pattern and no cusp because |**M** - 1| = 0 and **k** = -1; it is equivalent to a $\phi = 180°$ See Figure 2.4.3.
Figure 5.3.1. in which **M** =1.1, the scan pattern spirals into its center after five rotations. Thence it spirals outwards.
Figure 5.3.2. through 5.4.3. in which the scan patterns have non integral values of **M**. With **N** = 10 the scan patterns rotate through 10 cycles. Because the patterns repeat themselves whenever the product |**M***N| is an integer the irradiance of the pattern decreases towards the center of the doughnut shape of the scan patterns. The value of **M** needs to have a number with a recurring decimal for a smooth irradiance gradient with a high value for **N**.
It will again be observed that the number of cusps **C** is one digit less than the value of **M**, that is, **C** = |**M**-1|.

3.5. "Internal" polygons

In each of the uppermost six subFigures **M** ranges integrally from 1 through 6, while $\mathbf{k} = [-1]^{\mathbf{M}}(1/\mathbf{M})^2$. Mathematical analysis shows that poorly defined polygons are formed when $\mathbf{k} = [-1]^{\mathbf{M}}(1/\mathbf{M})^2$.

M = 1, 2, 3,
4, 5, 6

$\phi = 0°$

k = -1, +0.25, -0.11•
0.625, -0.04, 0.0277•

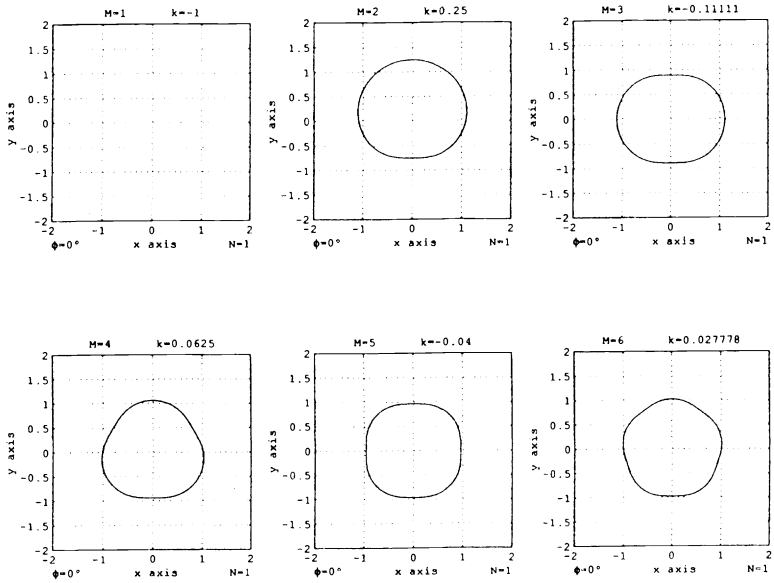

N = 1

M = 1.1, 2.2, 3.3
4.4, 5.5, 6.6

$\phi = 0°$

k = -1, +0.25, -0.11•
0.625, -0.04, 0.0277•

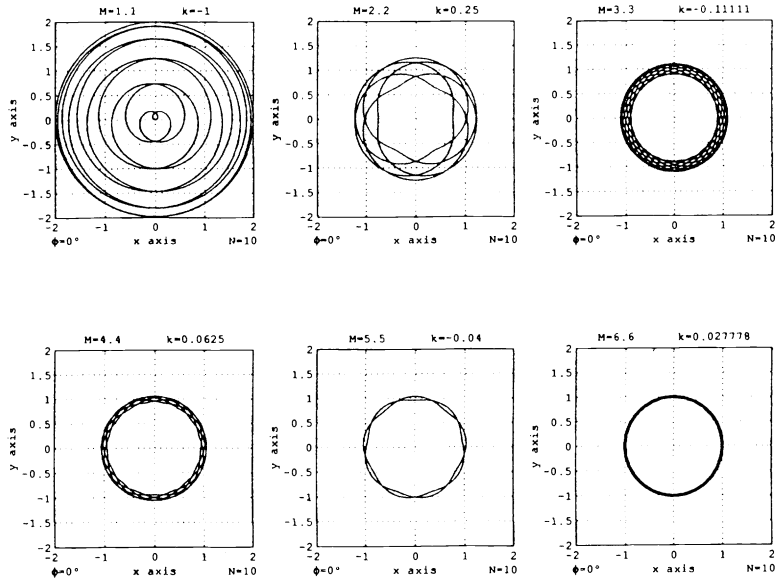

N = 10

Figure 6. In each of the lowermost six subFigures **M** is increased by 10% to range non integrally from 1.1 through 6.6.
Figure 6.1.1. has no scan pattern and no cusp because **M** = 1 and **k** = -1, the latter being equivalent to a phase change of 180° had **k** = +1. See Figure 2.4.3.
Figure 6.3.1. in which **M** =1.1, the scan pattern spirals into its center after five rotations. Thence it spirals outwards.
Figure 6.3.2. through 6.4.3. in which the scan patterns have non integral values of **M**. With **N** = 10 the scan patterns rotate through 10 cycles. Because the patterns repeat themselves whenever the product |**M***N| is an integer the uniformity of the irradiance gradient is difficult to assess qualitatively as the scan patterns have a thin ring shape. Compare with Figure 11.
It will again be observed that the number of facets **F** is one digit less than the numerical value of **M**, that is, **F** = |**M**-1|.

4. NEGATIVE VALUES OF M

Figures 7. through 11. only exhibit negative values of the ratio **M**; this means that Prism 2 is contrarotating with respect to Prism 1. **N** still represents the number of complete rotations of Prism 1.

4.1. Ellipses

M = -1

k = +0, +0.5, +1

$\phi = 0°$

$\phi = 45°$

$\phi = 90°$

$\phi = 180°$

N = 1

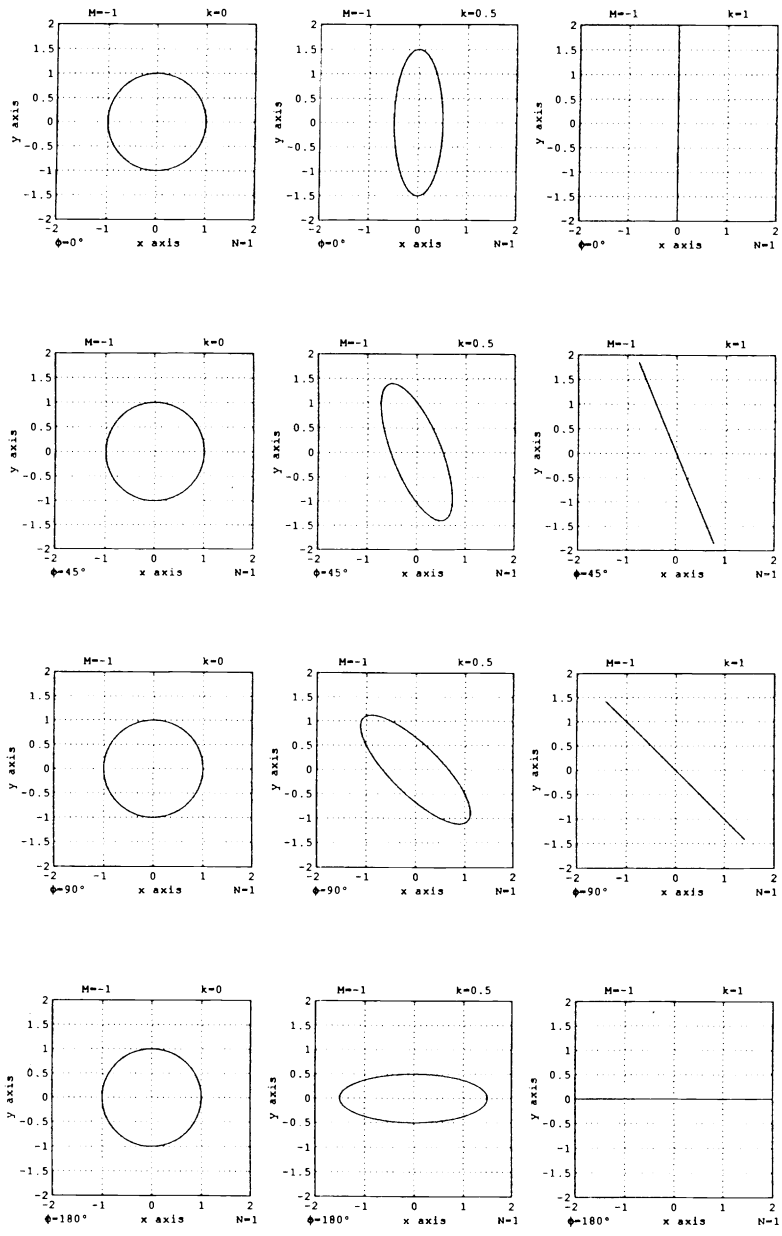

Figure 7. The four rows show the effect of changing the phase ϕ, from zero degree, 45°, 90°, 180°.
The three columns of Figure 7. show the the effect of changing the ratio **k** from zero, 0.5 and 1.0. **N**=1.
Column 1 depicts subFigures that are identical because **k**= zero. In effect Prism 2 is simply a parallel window that produces no angular deviation although it may produce displacement of the emergent beam according to the thickness of the window.
Column 2 depicts subFigures, for **k**= +0.5, of elliptical scan patterns that are reoriented as the phase ϕ increases.
Column 3 depicts subFigures, for **k**= +1, of straight line elliptical scan patterns that are reoriented as the phase ϕ increases to 180°. Compare with Figure 2.

4.2. External Loops

The upper set of six subFigures depicts scan patterns for integral steps of **M**, ranging from **M** = -1 through -6. The number of internal loops is in direct proportion to the numerical value of |**M**-1|. The size of the external loops depends on the value of **k**. Compare with Figure 3.

M = -1, -2, -3, -4, -5, -6

$\phi = 0°$

k = 0.7

N = 1

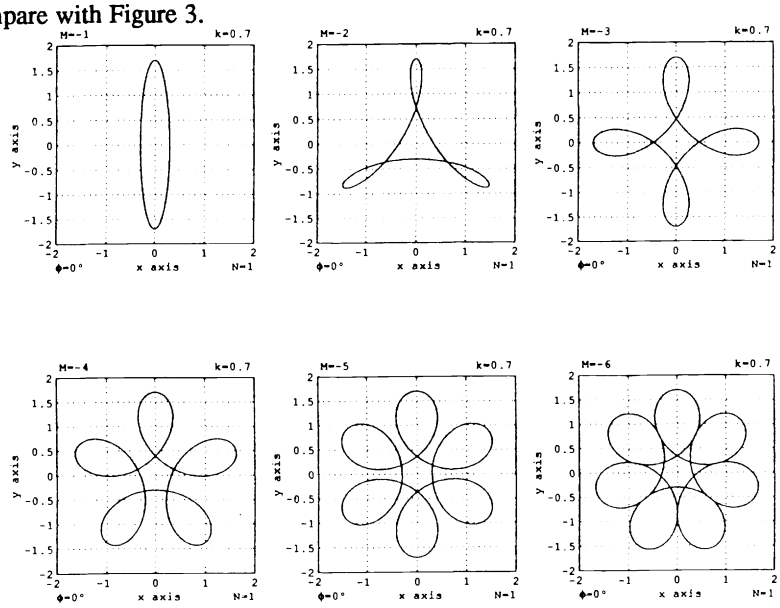

M = -1.1, -2.1, -3.1, -4.1, -5.1, -6.1

$\phi = 0°$

k = 0.7

N = 5

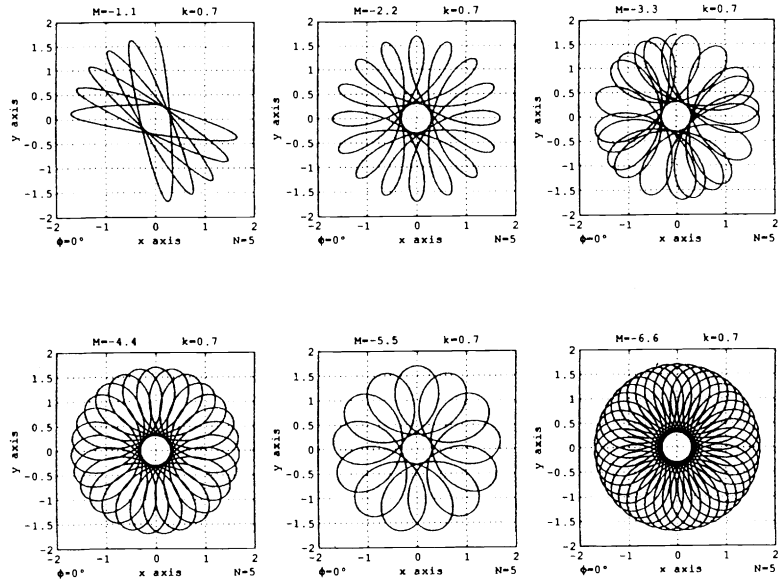

Figure 8. In each of the lowermost scan patterns **M** is increased by 10% to range non integrally from 1.1 through 6.6. Figures 8.3.1 through 8.4.3 with scan pattern have non integral values of **M**. With **N** = 5 the scan patterns rotate through **N** cycles. Because the patterns repeat themselves whenever the product |**M***N| is an integer the irradiance of the pattern increases towards the center of the doughnut shape of the scan patterns. The value of **M** needs to have a number with a recurring decimal for a smooth irradiance gradient.

It will be observed that the number of loops **L** is one digit more than the numerical value of **M**, that is, **L** = |**M**-1|.

4.3. Evolution of external regular polycusps and polygons.

Polycusps are defined as two-dimensional geometrical figures that have multiple cusps.

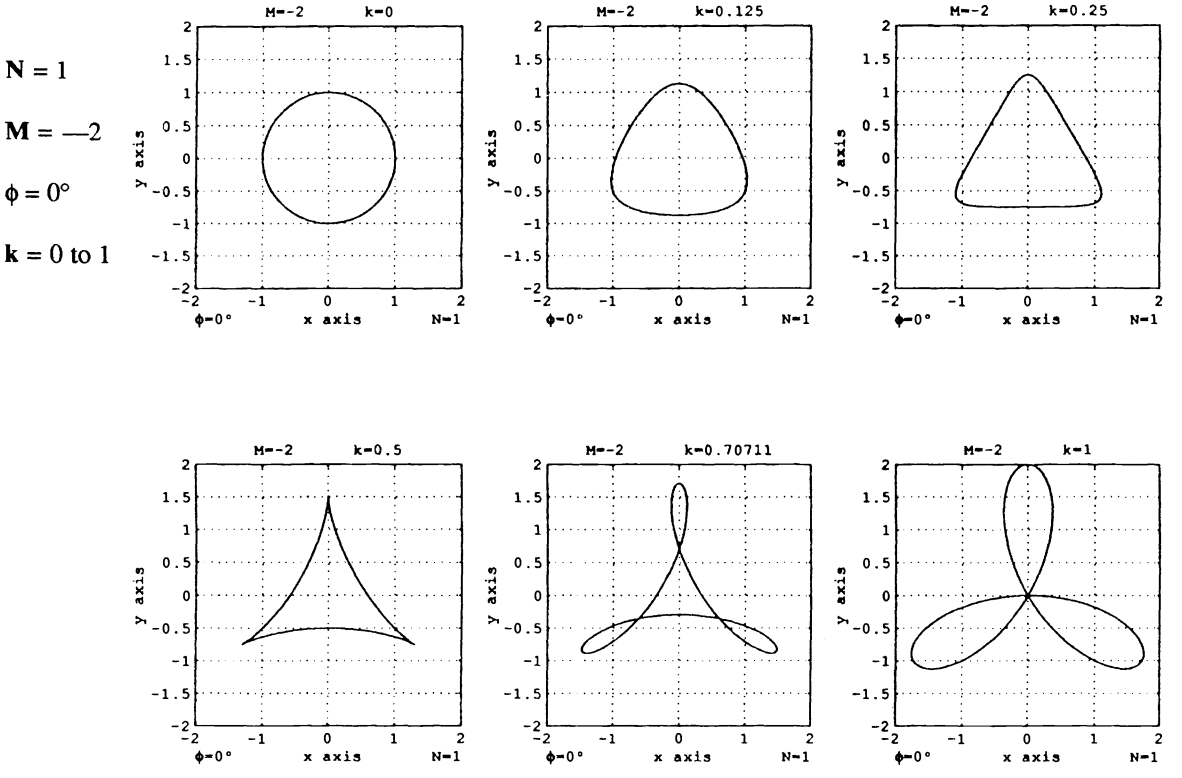

Figure 9. In each of the six subFigures **k** progressively ranges from zero to 1.

Figure 9.1.1. in which **k** = 0 the resultant scan pattern is understandably a circle as Prism 2 is simply a parallel window.

Figure 9.1.2. As **k** numerically increases the scan pattern changes to a bulging triangular shape.

Figure 9.1.3. As **k** continues to increase the scan pattern changes to a respectable triangle.

Figure 9.2.1. When **k** = 0.25 the resultant scan pattern has the distinct shape of an arrow head with three sharp external cusps. Thence in:

Figure 9.2.2. When **k** = 0.5 three external loops develop out of the cusps; the size of the loops depends on the value **k** > 0.5.

Figure 9.2.3. in which **k** = 1 the three external larger loops intersect at the center of the scan pattern. It will be noticed that the number of cusps **C** and loops **L** is one digit more than the numerical value of **M**, that is, **C** = **L** = |**M**-1| as in Figure 8. Mathematical analysis shows that internal cusps are formed when **k** =1/±**M**. Compare with Figure 4.

4.4. External regular polycusps

In each of the uppermost six subFigures **M** ranges integrally from 1 through 6, while $\mathbf{k} = [-1]^{M+1}(1/M)$.
The term $[-1]^{M+1}$ orients each subFigure scan pattern such that two cusps lie at the bottom about the centerline.

M = -1, -2, -3,
-4, -5, -6

$\phi = 0°$

k = -0.8, +0.5, -0.33•
0.25, -0.2, 0.166•

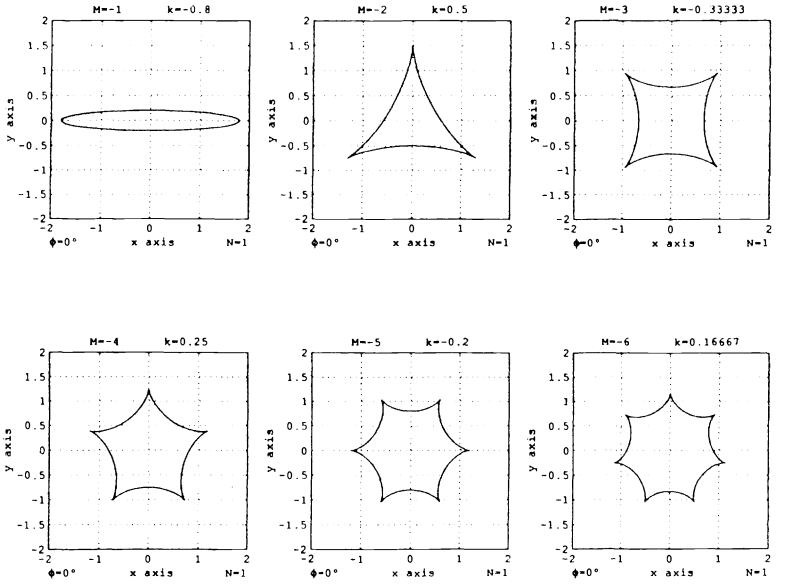

N = 1

M =- 1.1, -2.2, -3.3
-4.4, -5.5, -6.6

$\phi = 0°$

k = -0.8, +0.5, -0.33•
0.25, -0.2, 0.166•

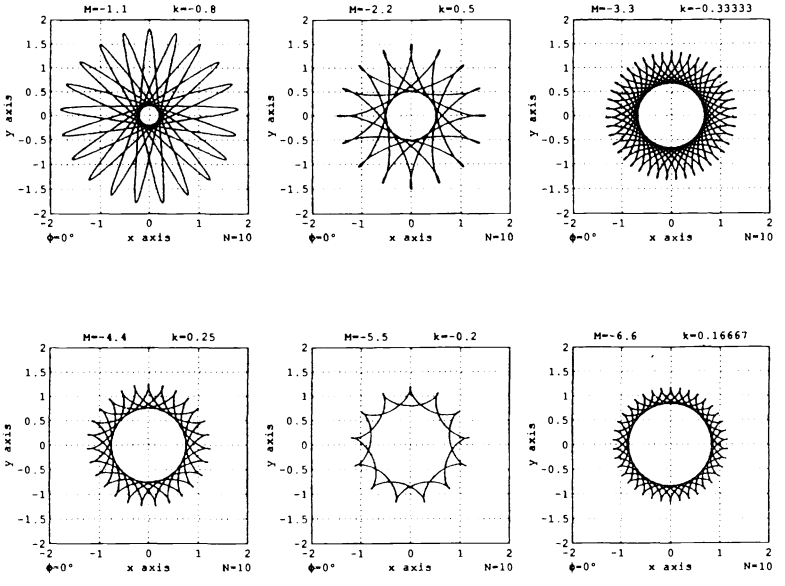

N = 10

Figure 10. In each of the lowermost six subFigures **M** is increased by 10% to range non integrally from 1.1 through 6.6.
Figure 10.1.1. scan pattern is an ellipse with no cusp because **k** = -0.8, instead of unity. If **k** = 1 the scan pattern would appear as a straight line, which theoretically may be considered to have two cusps, conforming to **C** = |**M**-1|.
Figure 10.3.1. the elliptical scan pattern rotates, leaving a hole in the center whose size depends on the the value of **k**.
Figure 10.3.2. through 10.4.3. in which the scan patterns have non integral values of **M**. With **N** = 10 the scan patterns rotate through 10 cycles. Because the patterns repeat themselves whenever the product |**M***N| is an integer the irradiance of the pattern increases towards the center of the doughnut shape of the scan patterns. The value of **M** needs to have a number with a recurring decimal for a smooth irradiance gradient with a high value for **N**.
It will be observed that the number of cusps **C** is one digit more than the numerical value of **M**, that is, **C** = |**M**-1|.

4.5. "External" regular polygons

In each of the uppermost six subFigures **M** ranges integrally from 1 through 6, while $\mathbf{k} = [-1]^{\mathbf{M}}(1/\mathbf{M})^2$. Mathematical analysis shows that more well defined polygons are formed when $\mathbf{k} = [-1]^{\mathbf{M}}(1/\mathbf{M})^2$.

M = -1, -2, -3, -4, -5, -6

$\phi = 0°$

k = -1, +0.25, -0.11•
0.625, -0.04, 0.0277•

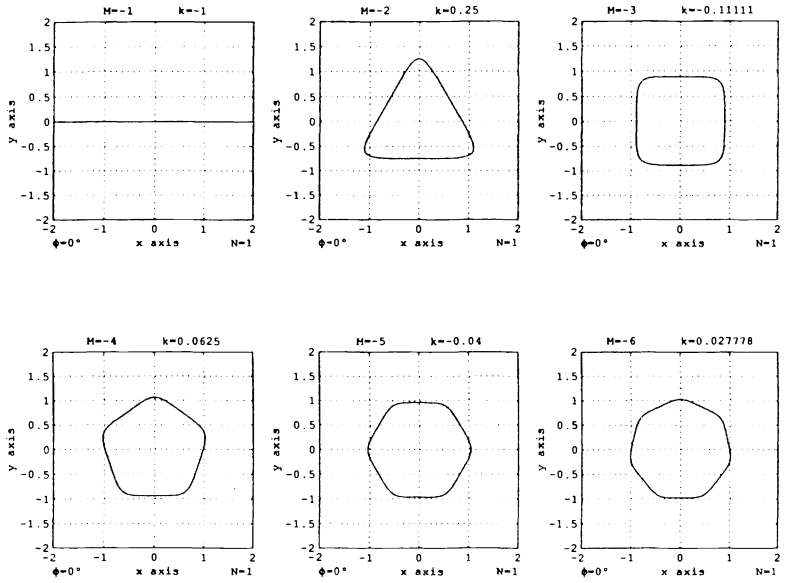

N = 1

M = -1.1, -2.2, -3.3 -4.4, -5.5, -6.6

$\phi = 0°$

k = -1, +0.25, -0.11•
0.625, -0.04, 0.0277•

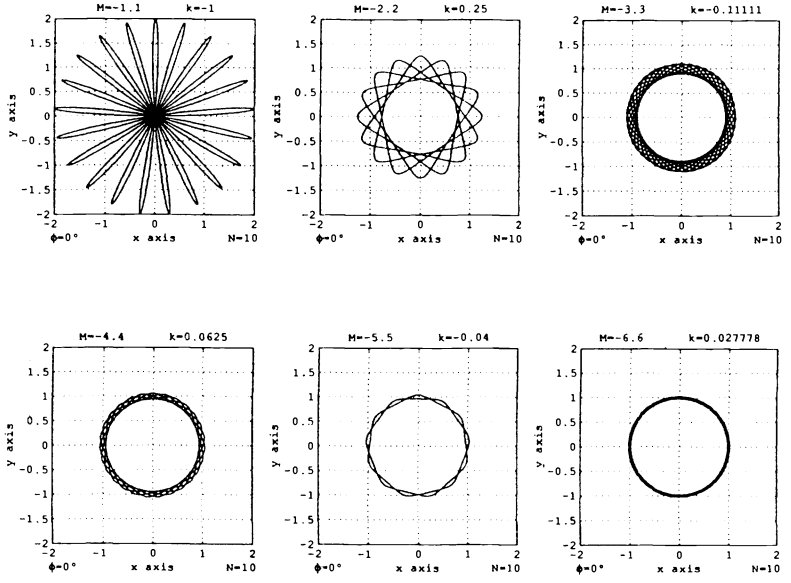

N = 10

Figure 11. In each of the lowermost six subFigures **M** is increased by 10% to range non integrally from 1.1 through 6.6.
Figure 11.1.1. has a scan pattern that is a straight line because **M** = 1 and **k** = -1, the latter being equivalent to a phase change of 180° had **k** = +1. See Figure 7.4.3. Theoretically the line is an ellipse whose minor diameter is zero.
Figure 11.3.1. in which **M** =1.1, has a rotating narrow elliptical scan pattern in the shape of a star with no hole at the center.
Figure 11.3.2. through 11.4.3. in which the scan patterns have non integral values of **M**. With **N** = 10 the scan patterns rotate through 10 cycles. Because the patterns repeat themselves whenever the product |**M***N| is an integer the uniformity of the irradiance gradient is difficult to assess qualitatively as the scan patterns have a thin ring shape. Compare with Figure 6.
It will again be observed that the number of facets **F** is one digit more than the numerical value of **M**, that is, **F** = |**M**-1|.

5. IMPLEMENTATION

Implementation may be achieved in at least two ways.

5.1. Nutating mirrors

Two nutating mirror scanners, which are slightly offset to avoid obscuration of the beam, will generate Risley scan patterns that are slightly asymmetrical.

5.2. Two Risley Prisms

The ratio **k** of the rotation speed of the wedges is easy to change and control. This is not so for the ratio **M** of the refracting angles of solid glass prisms.

5.2.1. Fine tuning of M

The more elegant way to readily implement the required prism power of the wedge prisms is to have two Risley prisms in tandem; each Risley prism being a sandwich of two wedge prisms whose orientation to each other can be adjusted to produce the required effective refracting angle (prism power) and, thereby, fine tune the ratio value of **M**.

5.3. Applications

There are probably a number of applications; several that come to mind are; the fields of dermabrasion, ophthalmology and "entertainment".

6. SUMMARY

The scan patterns that can be generated by a Risley optical scanning system, when suitable values of **M**, **k**, **N** and ϕ are chosen, are interesting and have several possible applications.

6.1. Special relationship between k and M

The most interesting discovery of the analysis is the ability to generate regular cuspidate and polygonal scan patterns when the value of **k** is expressed by $\mathbf{k} = 1/\mathbf{M}$ and $\mathbf{k} = 1/\mathbf{M}^2$ respectively. I have yet to explore $\mathbf{k} = 1/\mathbf{M}^m$, in which m is is variable exponent, to see what scan pattern it will generate (Figures 9. and 10.).

6.2. Positive and negative values of M

It is further interesting to note that the number of loops, cusps and facets equate to the numerical value of $|\mathbf{M}-1|$.

6.3. Future analysis

The sharpening of the corners of the polygonal scan patterns is a challenging analytical problem. I believe it may well be possible by having more than two Risley Prisms in series, each having their own multiple values of **k** and **M** between each combination of the Risley Prisms. This belief comes from the similarity of the problem with Fourier analysis. The more harmonic sinusoidal wave patterns are added at the correct phase to the fundamental wave; the sharper one can approximate to a square wave pattern.

7. ACKNOWLEDGEMENTS

I thank Mr Eric Pepper of SPIE for providing a reference; Mr. Stephen F. Sagan of Optical Research Associates Inc. for reviewing my manuscript; and Mrs Irene M. Marshall for proof reading the draft manuscript.

8. REFERENCES

1. Francis A. Jenkins and Harvey E. White, *Fundamentals of Optics*, Second edition, p. 31, 1951.
2. William L. Wolfe, Introduction to Infrared System Design, Second Printing, Tutorial Texts in *Optical Engineering* Vol. TT24, Donald C. O'Shea, Series Editor, SPIE Press, Bellingham, Washington. p. 85, 1996.